

Sensitivity of WallDYN material migration modeling to uncertainties in mixed-material surface binding energies



J.H. Nichols^{a,*}, M.A. Jaworski^a, K. Schmid^b

^aPrinceton Plasma Physics Laboratory, MS 30 C-Site, Princeton, NJ 08543, USA

^bMax-Planck-Institut für Plasmaphysik, Garching, Germany

ARTICLE INFO

Article history:

Received 15 July 2016

Revised 26 November 2016

Accepted 10 January 2017

Available online 9 March 2017

ABSTRACT

The WallDYN package has recently been applied to a number of tokamaks to self-consistently model the evolution of mixed-material plasma facing surfaces. A key component of the WallDYN model is the concentration-dependent surface sputtering rate, calculated using SDTRIM.SP. This modeled sputtering rate is strongly influenced by the surface binding energies (SBEs) of the constituent materials, which are well known for pure elements but often are poorly constrained for mixed-materials. This work examines the sensitivity of WallDYN surface evolution calculations to different models for mixed-material SBEs, focusing on the carbon/lithium/oxygen/deuterium system present in NSTX. A realistic plasma background is reconstructed from a high density, H-mode NSTX discharge, featuring an attached outer strike point with local density and temperature of $4 \times 10^{20} \text{ m}^{-3}$ and 4 eV, respectively. It is found that various mixed-material SBE models lead to significant qualitative and quantitative changes in the surface evolution profile at the outer divertor, with the highest leverage parameter being the C-Li binding model. Uncertainties of order 50%, appearing on time scales relevant to tokamak experiments, highlight the importance of choosing an appropriate mixed-material sputtering representation when modeling the surface evolution of plasma facing components. These results are generalized to other fusion-relevant materials with different ranges of SBEs.

© 2017 The Authors. Published by Elsevier Ltd.

This is an open access article under the CC BY-NC-ND license.

(<http://creativecommons.org/licenses/by-nc-nd/4.0/>)

1. Introduction

The erosion, migration, and redeposition of wall materials is a continuing issue facing current and future fusion devices, limiting the lifetime of plasma facing components (PFCs) in net erosion regions and providing an impurity source that can degrade core plasma performance. This issue becomes even more complex in tokamak environments that utilize multiple wall materials. Mixed-material compounds and alloys that form due to material migration can exhibit different structural properties than their constituent elements, and the sputtering behavior of such mixed materials may be poorly understood [1]. Furthermore, hydrogen can be codeposited in significant quantities in redeposited material layers, leading to concerns about exceeding tritium inventory limits [2].

Mixed materials are of special importance in the National Spherical Torus Experiment (NSTX), which had PFCs made of ATJ

graphite (and molybdenum in select campaigns) but regularly introduced elemental lithium to improve plasma performance [3]. As the suitability of solid and/or liquid lithium PFCs is evaluated for future fusion devices, it is critical to understand the makeup of the mixed materials that Li forms with its substrate and other impurities, and whether these mixed materials still contribute to plasma performance in a positive way.

Ideally, the modeling of mixed-material wall evolution due to tokamak plasma-material interactions would be accomplished by coupling advanced molecular dynamics (MD) surface codes with well-established plasma models. However, this is computationally intractable due to the wide range of length scales (\sim nm surface processes vs. \sim 10 m machine size) and time scales (\sim μs plasma fluctuations vs. \sim 100 s discharge length) involved. To get around this, the WallDYN code [4, 5] was developed to self-consistently model the material erosion/transport/deposition/re-erosion/re-deposition steps that shape the evolution of PFC composition and impurity influx. WallDYN does this by parameterizing the output of impurity transport models and surface process models into rate equations, which feed into a system of differential-algebraic equations that describe the impurity influx/outflux and

* Corresponding author.

E-mail address: jnichols@pppl.gov (J.H. Nichols).

the surface areal density at every wall location. These equations are described in detail in [4] and [5], and the results have been validated against beryllium [6] and tungsten [7] migration experiments in JET.

This work presents the first application of the WallDYN model to the NSTX geometry, and demonstrates the sensitivity of WallDYN results to key assumptions in the surface model. A plasma background is generated for an NSTX H-mode discharge, and the Monte Carlo impurity transport code DIVIMP [8] is used to parameterize the redistribution of carbon, lithium, and oxygen. A parameterized surface model describing composition-dependent sputtering and reflection is generated using the binary collision approximation (BCA) code SDTRIM.SP [9,10]. Special focus is paid to the mixed-material surface binding energies (SBEs) utilized inside SDTRIM.SP, including the effect these have on WallDYN calculations.

2. Plasma model

The plasma background used in this study is reconstructed using inter-ELM data from NSTX discharge 139,396 at 600 ms, a lower single null, low-triangularity, H-mode plasma with $B_t = 0.45$ T, $I_p = 0.8$ MA, $P_{NBI} = 4$ MW, $\langle n_e \rangle = 6.5 \times 10^{21} \text{ m}^{-3}$, and $B \times \nabla B$ drift toward the x-point. The outer strike point was located on the Liquid Lithium Divertor (LLD), operated in unheated mode such that the lithium surface remained solid throughout the discharge. Radial profiles of outer target temperature and ion saturation current are obtained using the High Density Langmuir Probe (HDLP) array [11]. Measured outer divertor target parameters are $n_e = 0.3\text{--}4 \times 10^{20} \text{ m}^{-3}$ and $T_e = T_i = 2\text{--}5$ eV. A more complete discussion of this discharge can be found in [12]. The high energy electron tail reported in [12] is ignored in this analysis due to its small contribution to erosion in comparison to the bulk population. Erosion due to edge localized modes (ELMs) is also neglected in this analysis, since gross erosion in NSTX is dominated by inter-ELM physical and chemical sputtering of the low-Z PFC materials. Note that this assumption does not hold for high-Z machines, where sputtering by hot ions present during an ELM can be the dominant erosion mechanism [7].

n_e , T_e , T_i , and background flow profiles for this discharge are shown in Fig. 1, and are calculated using the quasi-1D ‘Onion Skin Model’ (OSM) option in DIVIMP [13], which simultaneously solves four fluid conservation equations (particle, ion and electron power, and momentum) along flux surface-aligned rings with a 5th-order Runge–Kutta method. Langmuir probe data are used as a boundary condition for each ring, and solutions are iterated with the hydrogenic neutral Monte Carlo code EIRENE [14] to provide accurate ionization, power, and momentum source terms. Plasma parameters inside the last closed flux surface are set using data from Thomson scattering and charge exchange recombination spectroscopy. NSTX lacked reliable Langmuir probe data for the inner divertor leg, so in this study the focus will be behavior at the outer divertor. Outer divertor data are mirrored to the inner divertor so as to provide a plausible (though not fully validated) plasma solution for the entire SOL. In this case, OSM calculates excess ionization in the hot regions of the SOL nearest the separatrix, leading to flow reversal. While this feature has a significant impact on impurity transport in the SOL, experimental validation is difficult and thus an in-depth analysis of its physicality is left for future work.

In this study, the physical NSTX wall is replaced by a model wall that closely surrounds the computational grid. The reasoning for this is that grid limitations currently prevent the computational grid from reaching the actual wall, but short-range transport is a critical component of the redistribution chain and thus must be resolved accurately on the grid. Work is ongoing to incorporate “extended” grids, which fill the remaining far SOL with short flux

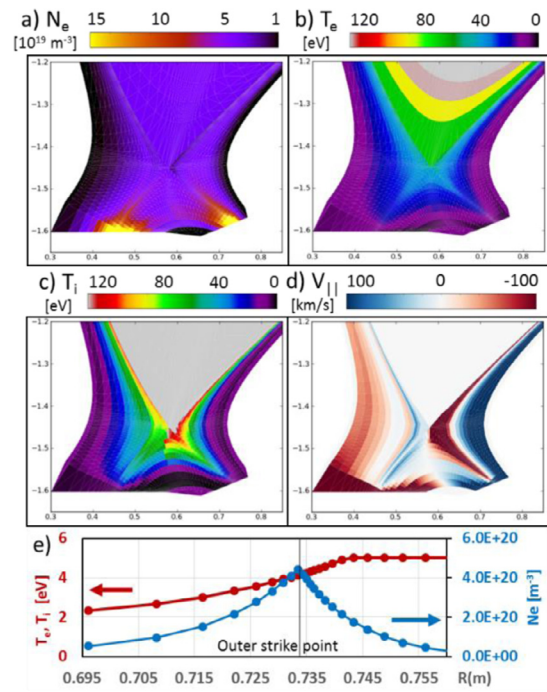


Fig. 1. Divertor plasma reconstructions for 139,396, calculated by OSM: (a) electron density; (b) electron temperature; (c) ion temperature; (d) deuterium flow velocity parallel to B, positive is towards the outer divertor; (e) outer target temperature and density Langmuir probe data vs. radius, input to OSM.

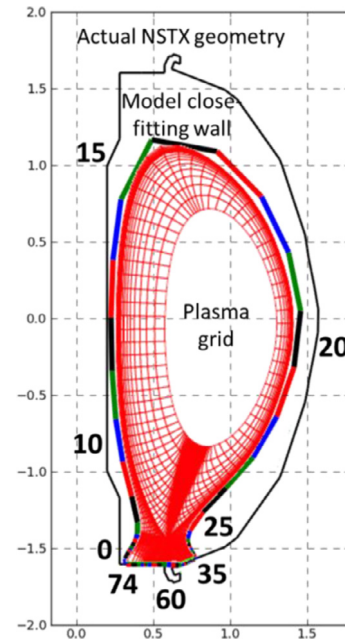


Fig. 2. Model wall, closely fitting the plasma grid, partitioned into 75 bins. Bins 0–34 represent the main wall; bins 35–58 the outer target; bins 59–63 the private flux zone; bins 64–74 the inner target. The actual NSTX wall geometry is shown for reference.

tubes, into the NSTX WallDYN workflow to remove the necessity of this assumption. This model wall is discretized into 75 bins, as seen in Fig. 2, with the highest resolution at the outer divertor. Wall binning was set up such that the grid spacing at the outer divertor is smaller than local ionization mean free paths.

Deuterium ion and neutral fluxes to the wall are assumed to be static, and are taken from the final EIRENE iteration. Fluxes of the wall material impurities (C and Li) are dynamic, and depend on the

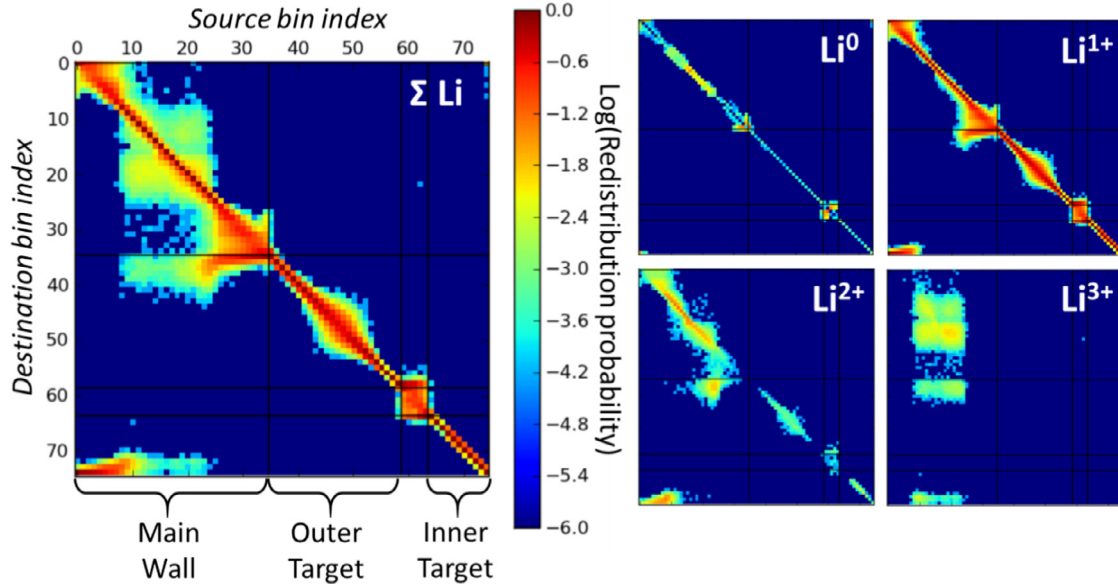


Fig. 3. Charge-integrated Li redistribution matrix calculated by DIVIMP. A particle launched from the source bin has the given probabilities of redepositing on each destination bin. Inset: Charge-resolved Li redistribution matrices, showing the probability of an initially neutral atom depositing in a given charge state.

instantaneous state of the PFC surface. Oxygen is also treated as a dynamic flux, since it is a common impurity in NSTX and plays an important role in C-Li surface chemistry [15]. The trace impurity code DIVIMP is used to calculate the probability that a neutral particle launched from one bin ends up depositing, as a specific charge state, on any of the other bins in the simulation. Continuing this for all bins in the system maps out a source-destination redistribution matrix that fully characterizes impurity transport for a given element. Fig. 3 shows the redistribution matrices for all charge states of Li, as well as the charge-integrated matrix. The highly diagonal nature of the matrix confirms that multiple short-range redistribution steps are the dominant mechanism for moving material around a tokamak. Also evident are horizontal bands corresponding to long-range transport from the walls to the divertor targets. The redistribution matrices for C and O are qualitatively similar to Li, though slightly broader due to the increased ionization mean free paths for these elements.

3. Surface model

Composition-dependent rate equations for sputtering and reflection are generated using SDTRIM.SP version 5.07 [9,10]. Parameter scans are performed across a full range of incident energies/species and surface composition, using a KrC interaction potential and a 40° from surface normal angle of incidence (to model the straightening of ions in the magnetic presheath [16]). Physical sputtering rates for each projectile/substrate combination are then fit to a Bohdansky-like formula [17] with added composition dependence:

$$Y_{sput}^{FIT} = Q * s_n(E_0/E_{TF}) * (1 - (E_{th}/E_0)^{2/3}) * (1 - E_{th}/E_0)^2 * (1 + \sigma_c a_c + \sigma_{Li} a_{Li} + \sigma_o a_o).$$

Here E_0 is the incident energy, s_n the nuclear stopping potential, and E_{TF} the Thomas-Fermi energy. Q and E_{th} are the familiar Bohdansky fitting parameters, while σ_n is the areal density of element n and a_n is the corresponding fitting parameter. Likewise, reflection yields are fit to a modified power law formula:

$$Y_{refl}^{FIT} = \rho_{refl} * E_0^\alpha * (1 + \sigma_c b_c + \sigma_{Li} b_{Li} + \sigma_o b_o).$$

Here ρ_{refl} and α are the energy fitting parameters, and b_n are the composition fitting parameters. These functions are capable of robustly fitting SDTRIM.SP results, typically matching Y_{sput} within 10% and Y_{refl} within 30%. Chemical sputtering is included for D on C, using the formulae of Roth [18] and scaling the yield linearly with the surface C concentration.

The key variable inside SDTRIM.SP examined in this study is the surface binding energy (SBE). Computationally, the SBE is the energy, specific to a surface, which a perpendicular recoil atom must exceed in order to trigger a sputtering event. For pure materials, it has been found that the sublimation energy of an element is a good model for its SBE. However, SBEs for mixed materials are poorly characterized and thus approximations are generally made. Following Eckstein [19], we examine 3 models for effective mixed material SBEs involving elements with pure SBEs SBE_1 and SBE_2 : (1) composition-independent, $SBE_{1,eff} = SBE_1$; (2) linearly composition-dependent, $SBE_{1,eff} = q_1 SBE_1 + q_2 SBE_2$; (3) linearly composition-dependent between pure and average SBEs, $SBE_{1,eff} = q_1 SBE_1 + q_2 (SBE_1 + SBE_2)/2$. In previous studies Walldyn has utilized model 3, though in this work we emphasize the other two more extreme models so as to maximize the potential effect on results.

For the three-element environment of NSTX, the surface binding energy takes the form of $SBE_{i,eff} = \sum_j q_j * SBE_{i,j}$, where q_j is again the concentration of element j . $SBE_{i,j}$ takes the form of the well-known sublimation energy ($SBE_{Li-Li} = 1.64$ eV, $SBE_{C-C} = 7.37$ eV, $SBE_{O-O} = 2.58$ eV). To test SBE model 1, we perform one run where $SBE_{i,eff} = SBE_{i,j}$, independent of composition. To test model 2, we further assume that mixed material SBEs affect each element the same, i.e. $SBE_{i,j} = SBE_{j,i}$. The parameter space can then be filled with 8 permutations, with SBE_{Li-C} , SBE_{Li-O} , and SBE_{C-O} alternating between the pure SBEs of the constituent elements. New sputtering rate equations are fit for each case, and Walldyn is run using otherwise identical conditions.

4. Results and discussion

The initial state of all PFC surfaces in each simulation are treated as a 40 angstrom thick homogenous layer, with atomic composition 80% Li, 10% C, and 10% O (consistent with post-

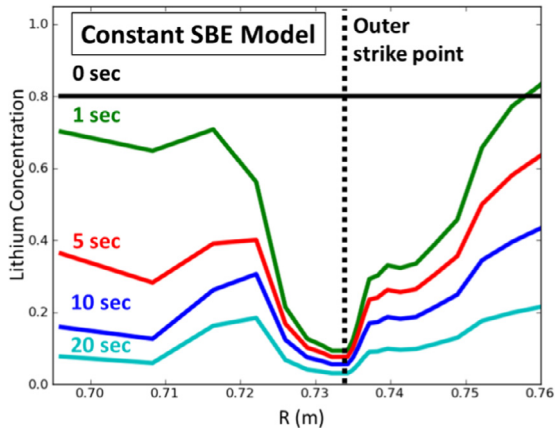


Fig. 4. Li concentration profiles vs. major radius near the outer strike point, calculated using the constant SBE surface model. Profiles are shown after 0, 1, 5, 10, and 20 s of plasma exposure. The outer strike point for this equilibrium is located at $R = 73.4$ cm.

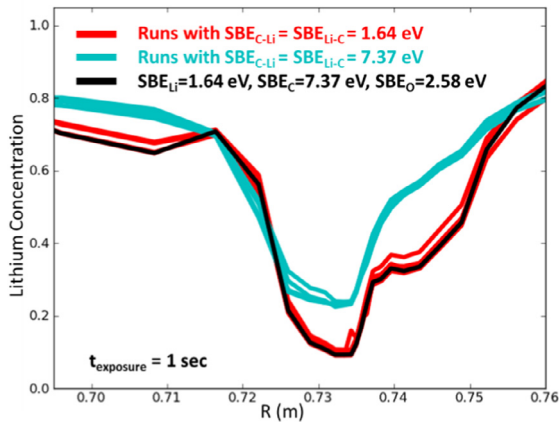


Fig. 5. Calculated Li concentration vs. major radius near the outer strike point, after 1 s plasma exposure. Runs with similar C-Li SBE coupling terms are grouped by color. (For interpretation of the references to color in this figure legend, the reader is referred to the web version of this article.)

evaporation data from the Material Analysis and Particle Probe [20]), on top of an infinite bulk of pure C. Diffusive and temperature-dependent surface processes are neglected in this analysis for simplicity.

Fig. 4 shows the time evolution of Li concentration in the vicinity of the outer strike point, using the concentration-independent SBE model. One second of plasma exposure corresponds approximately to one NSTX discharge. The rapid depletion of Li from the strike point, followed by depletion of Li from the rest of the outer divertor, is consistent with ion beam analysis [21] and qualitative post-vent visual observations from NSTX. All SBE models show this characteristic migration of Li from the strike point, but the quantitative behavior differs significantly. The Li concentration profiles after one second of plasma exposure for all SBE models are shown in Fig. 5, and there is a clear demarcation between the behavior of models with $SBE_{Li-C} = SBE_{C-Li} = 1.64$ eV and $SBE_{Li-C} = SBE_{C-Li} = 7.37$ eV. This correlation with SBE_{Li-C} persists as exposure times increase, though SBE_{Li-O} appears as a subdominant sorting variable after 20 s exposure. But is SBE_{Li-C} or SBE_{C-Li} the variable that is driving the primary bifurcation? If SBE_{C-Li} was the key variable, then the constant SBE model would track with $SBE_{Li-C} = SBE_{C-Li} = 7.37$ eV, since both would have $SBE_{C,eff} \approx 7.37$ eV. However, it is clear that the constant SBE model tracks with $SBE_{Li-C} = SBE_{C-Li} = 1.64$ eV, meaning that SBE_{Li-C} is the controlling variable. The two classes of profiles show the same primary qualitative behavior, in that the Li con-

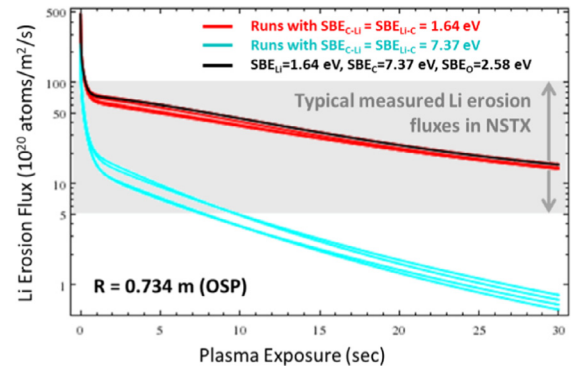


Fig. 6. Calculated Li erosion flux vs. plasma exposure, at the outer strike point. Runs with similar C-Li SBE coupling terms are grouped by color. The gray band signifies the scale of typical Li erosion flux measurements in NSTX [21]. (For interpretation of the references to color in this figure legend, the reader is referred to the web version of this article.)

centration decreases near the strike point, but differ in secondary qualitative behavior such as lobe and profile shape. Also, there is an order 50% difference in the quantitative Li concentration calculated at the strike point itself over all exposure time scales.

It is important to note that the Li erosion fluxes also segregate strongly with SBE model, since these are closer to what is measured by spectroscopic diagnostics in tokamaks. Fig. 6 shows the time evolution of the flux of Li eroded from the outer strike point for all simulations, again grouped according to $SBE_{C-Li} = SBE_{Li-C}$. As expected, erosion fluxes are higher in the cases in which Li atoms are less strongly bound by the mixed material. However, what is striking is the magnitude of the difference between the two sets of models, which differ by a factor of 5–20 after one second of plasma exposure. Also plotted in Fig. 6 is a range of “typical” Li erosion fluxes for NSTX, measured spectroscopically at a range of locations on the outer target and for a range of plasma configurations [22]. We see that these initial WallDYN simulations are generally the right order of magnitude for Li erosion, though they may underestimate erosion when using the most strongly bound mixed material models. These simulations also overestimate erosion in the first 0.5 s of exposure, likely signifying that the real PFC surface contains less than 80% Li. A quantitative comparison to spectroscopic erosion data would require that careful attention be paid to the initial state of the PFC surfaces, as well as evolving the simulated D^+ and D^0 flux to match the observed intra-discharge density evolution. While this comparison is planned for NSTX-U, it is beyond the scope of this paper.

It is also instructive to examine the evolution of the O concentration profile in the same region, as seen in Fig. 7. Once again we see a clear grouping of profiles that persists through all exposure times, though with more relative spread due to the comparatively low O concentration. This time, the profiles correlate with $SBE_{C-O} = SBE_{O-C}$. Since the constant SBE model follows $SBE_{C-O} = SBE_{O-C} = 2.58$ eV, we can conclude that SBE_{O-C} is the controlling variable for the O concentration evolution.

Since the initial surface layer in this simulation is primarily Li, and the bulk is pure C, it is perhaps natural that how the Li sputtering rate is modified by increasing C concentration is the determining factor for the evolution of the system. However, since the O concentration evolution depends on the modification of SBE_O by C even when the Li concentration exceeds the C concentration, this is not purely a composition effect. Instead, the observed behavior is likely due to the specific SBE values of the elements involved in the system. Li (1.64 eV) and O (2.58 eV) both have low pure SBEs, meaning that different SBE models won't have a large effect on SBE_{eff} . Meanwhile, the large SBE of pure C (7.37 eV) means that C

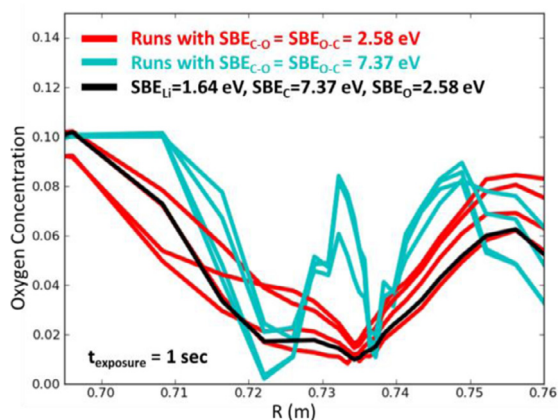


Fig. 7. Calculated O concentration vs. major radius near the outer strike point, after 1 s plasma exposure. Runs with similar C-O SBE coupling terms are grouped by color. (For interpretation of the references to color in this figure legend, the reader is referred to the web version of this article.)

can have an outsized effect on the SBE_{eff} of the other materials, depending on the SBE model used. Looking at the SBEs of other fusion-relevant materials (W: 8.79 eV, Mo: 6.81 eV, Be: 3.31 eV), it is likely that the choice of SBE models will be important for WallDYN calculations whenever there is a mix of high- and low-SBE materials, such as Mo+Li in NSTX-U or W+Be in JET-ILW, but less important for something like C+W in DIII-D.

Obviously, a linear SBE model may not accurately capture all of the physics present in a complex mixed-material system. For example, it has been shown that Li rapidly diffuses into C [23], that the Li sputtering yield exhibits strong temperature dependence [24,25,26], and that D implantation can markedly decrease the gross sputtering yield of Li [26]. Since D implantation is not accounted for in this simulation, the Li erosion rates used in this work likely serve as an upper bound. Additionally, the formation of compounds may mean that a non-linear composition dependence is more appropriate for the SBE, and this dependence may change case-by-case. These effects likely need to be considered when making a quantitative comparison between simulation and experiment. However, it is clear that in many fusion-relevant applications, the SBE model alone can be responsible for variations of order 50% in the concentration profiles calculated by WallDYN, and even greater changes in the calculated erosion fluxes. Thus, it is important to validate the SBE model against experimental data. For the case of NSTX, the most useful experiment is a well-controlled test stand setup to measure the binding energy of Li as a function of C concentration.

It is also important to consider how the uncertainty introduced by the mixed material SBE model compares to other uncertainties in the system. For instance, chemical sputtering is the dominant erosion mechanism for C in the NSTX divertor, and chemically sputtered C will have a different energy distribution compared to physically sputtered C. However, the results presented here are quite robust to different sputtered energy distributions, showing negligible changes when the Thompson distribution typically assumed in WallDYN is replaced with a 1 eV Maxwellian energy distribution that molecular dynamics simulations show is more representative of chemically sputtered C [27]. The reason for this is that in all cases C will redeposit within a few cm, and Li migration in the system is dominated by D->Li physical sputtering, and thus the presence or absence of high-charge state C ions (which are disproportionately born from the high-energy tail of the Thompson distribution) makes little difference. It is important to note that this will not be the case for main wall sputtering, where C redistribution will vary more widely depending on its energy distribution,

and for machines with high-Z materials, where sputtering can be dominated by high-charge state ions.

Since the yield curves for Li physical sputtering are rather steep at the low energies of the NSTX divertor, there is the potential for uncertainty due to the target conditions. However, these results are relatively robust to systematic errors in target density and temperature, since uniformly higher/lower erosion rates will obviously lead to higher/lower gross erosion but comparatively little change in net migration of material. On the other hand, changes in radial gradients in plasma parameters should have a significant effect on net migration, since it is the gradient of erosion rates that ultimately drives migration in stepwise transport systems. Still, even when maximizing gradients within the error bars quoted for the Langmuir probes, the uncertainty on the Li concentration profile is still less than that caused by SBE uncertainties.

5. Conclusions

Initial calculations with WallDYN have been performed on the NSTX system, with a dynamic mix of carbon, lithium, and oxygen on the PFCs. Rough qualitative agreement is observed with observed patterns of lithium depletion from the outer strike point on the time scale of a few discharges after an evaporation, and order-of-magnitude agreement with spectroscopic Li erosion data is observed while making certain assumptions within the SBE model, but not with others. Uncertainties of order 50% in concentration, and a full order of magnitude in erosion flux, can arise by using different, but reasonable, models for mixed material SBEs for the surface terms in WallDYN. In NSTX the most important variables are the modification of the Li and O SBEs by C, and in general the mixed material SBE model will be important when there is a large discrepancy between the SBEs of the constituent elements. This underscores the importance of verifying surface model assumptions with well-controlled test stand experiments.

Acknowledgments

The authors acknowledge useful discussions with G. Meisl, T. Abrams, F. Scotti, and R. Kaita. This work was supported by US-DOE contract DE-AC02-09CH11466, as well as EURATOM within the framework of the European Fusion Development Agreement.

References

- [1] G. Federici, et al., Nucl. Fusion 41 (2001) 1967.
- [2] J. Roth, et al., Plasma Phys. Control. Fusion 50 (2008) 103001.
- [3] R. Maingi, et al., Phys. Rev. Lett. 107 (2011) 145004.
- [4] K. Schmid, et al., J. Nucl. Mater. 415 (2011) S284–S288.
- [5] K. Schmid, et al., J. Nucl. Mater. 463 (2015) 66–72.
- [6] M. Reinelt, et al., J. Nucl. Mater. 415 (2011) S305–S309.
- [7] K. Schmid, et al., Nucl. Fusion 55 (2015) 053015.
- [8] P.C. Stangeby, et al., J. Nucl. Mater. 196–198 (1992) 258–263.
- [9] W. Moller, et al., Comput. Phys. Comm. 51 (1988) 355–368.
- [10] A. Mutzke, et al., IPP Report 12/8 (2011).
- [11] J. Kallman, et al., Rev. Sci. Instrum. 81 (2010) 10.
- [12] M.A. Jaworski, et al., J. Nucl. Mater. 438 (2013) S384–S364.
- [13] P.C. Stangeby, et al., J. Nucl. Mater. 313–316 (2003) 883–887.
- [14] D. Reiter, et al., Fusion Sci. Tech. 47 (2005) 172.
- [15] P.S. Krstic, et al., Phys. Rev. Lett. 110 (2013) 105001.
- [16] K. Schmid, et al., Nucl. Fusion 50 (2010) 025006.
- [17] J. Bohdansky, Nucl. Instrum. Meth. B 2 (1984) 587–591.
- [18] J. Roth, J. Nucl. Mater. 266–269 (1999) 51–57.
- [19] W. Eckstein, et al., Nucl. Instrum. Meth. B 119 (1996) 477–486.
- [20] M.J. Lucia, Material Surface Characteristics and Plasma Performance in the Lithium Tokamak Experiment PhD Thesis, Princeton University, 2015.
- [21] W.R. Wampler, et al., J. Nucl. Mater. 390–391 (2009) 1009–1012.
- [22] F. Scotti, Modifications of Impurity Transport and Divertor Sources by Lithium Wall Conditioning in the National Spherical Torus Experiment PhD Thesis, Princeton University, 2014.
- [23] N. Itou, et al., J. Nucl. Mater. 290–293 (2001) 281–285.
- [24] J.P. Allain, et al., Phys. Rev. B 76 (2007) 205434.
- [25] T. Abrams, et al., Fusion Eng. Des. 89 (2014) 2857–2863.
- [26] T. Abrams, et al., Nucl. Fusion 56 (2016) 016022.
- [27] J. Marian, et al., J. Appl. Phys. 101 (2007) 044506.